Size, Structure, and Helical Twist of Graphene Nanoribbons Controlled by Confinement in Carbon Nanotubes

Thomas W. Chamberlain,[†] Johannes Biskupek,[‡] Graham A. Rance,[†] Andrey Chuvilin,[§,⊥] Thomas J. Alexander,[†] Elena Bichoutskaia,[†] Ute Kaiser,[‡] and Andrei N. Khlobystov[†,*]

[†]School of Chemistry, University of Nottingham, University Park, Nottingham NG7 2RD, United Kingdom, [‡]Central Facility of Electron Microscopy, Group of Electron Microscopy of Materials Science, Ulm University, Albert-Einstein-Allee 11, D-89081 Ulm, Germany, [§]CIC nanoGUNE Consolider, Tolosa Hiribidea 76, E-20018, Donostia-San Sebastian, Spain, and [⊥]IKERBASQUE, Basque Foundation for Science, 48011, Bilbao, Spain

ABSTRACT

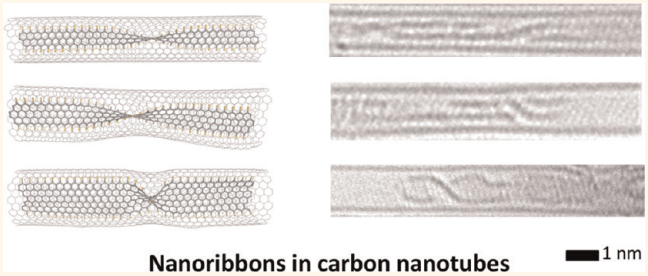

Carbon nanotubes (CNTs) act as efficient nanoreactors, templating the assembly of sulfur-terminated graphene nanoribbons (S-GNRs) with different sizes, structures, and conformations. Spontaneous formation of nanoribbons from small sulfur-containing molecules is efficiently triggered by heat treatment or by an 80 keV electron beam. S-GNRs form readily in CNTs with internal diameters between 1 and 2 nm. Outside of this optimum range, nanotubes narrower than 1 nm do not have sufficient space to accommodate the 2D structure of S-GNRs, while nanotubes wider than 2 nm do not provide efficient confinement for unidirectional S-GNR growth, thus neither can support nanoribbon formation. Theoretical calculations show that the thermodynamic stability of nanoribbons is dependent on the S-GNR edge structure and, to a lesser extent, the width of the nanoribbon. For nanoribbons of similar widths, the polythiaperipolycene-type edges of zigzag S-GNRs are more stable than the polythiophene-type edges of armchair S-GNRs. Both the edge structure and the width define the electronic properties of S-GNRs which can vary widely from metallic to semiconductor to insulator. The encapsulated S-GNRs exhibit diverse dynamic behavior, including rotation, translation, and helical twisting inside the nanotube, which offers a mechanism for control of the electronic properties of the graphene nanoribbon *via* confinement at the nanoscale.

KEYWORDS: carbon nanotube · graphene nanoribbon · nanoreactor · host–guest structure · aberration-corrected high-resolution transmission electron microscopy

While graphene is currently receiving significant attention because of the unique physical properties it exhibits, the absence of an electronic band gap in this material remains one of the main obstacles hindering its application in electronic devices. One of the most effective solutions for introducing an energy gap between the conduction and valence bands of graphene is to slice the 2D structure into strips of a fixed width—graphene nanoribbons (GNRs).[1−3] The discovery that the electronic properties of GNRs are highly dependent on the width and edge structure[4−11] of the ribbon has stimulated a significant recent wave of research to tailor the size and shape of GNRs.

Several approaches have been recently proposed, including "top-down" methods for GNR formation, such as the unzipping of carbon nanotubes or the cutting of graphene monolayers[4,5,7,12] by lithographic[13,14] or catalytic[15,16] methods. However, precise control of the GNR edge structure, which wholly defines the properties of the nanoribbon, still remains a significant challenge in such top-down methods.[17]

Recently, we reported the use of single-walled carbon nanotubes (SWNTs) as effective one-dimensional templates for the controlled self-assembly of GNRs.[18] Our method utilizes the relatively inert nature of the internal cavity of carbon nanotubes as a reaction vessel for the self-assembly of nanoribbons of uniform, well-defined structure (width ~ 1 nm), using carbon and sulfur building blocks generated *via* the thermal decomposition of simple molecular precursors inserted into the nanotube. In this study, we demonstrate that the formation of sulfur-terminated nanoribbons (S-GNRs) is a general, thermodynamically driven phenomenon. We introduce a methodology for controlling the width and the edge structure of S-GNRs by using nanoreactors (nanotubes) of different diameters. We determine the optimum range of nanoreactor diameters for GNR synthesis, thus opening a pathway for mass production of these nanostructures. Our theoretical calculations compare the relative stabilities of different types of nanoribbons and predict electronic

* Address correspondence to andrei.khlobystov@nottingham.ac.uk.

Received for review January 11, 2012 and accepted April 6, 2012.

Published online April 06, 2012
10.1021/nn300137j

properties ranging from metallic conductor to semiconductor to insulator, depending on the S-GNR edge structure.

RESULTS AND DISCUSSION

The process requires the introduction of a suitable carbon feedstock to form the GNR and a source of sulfur to terminate the dangling bonds and thus stabilize the edges of the GNR. The sulfur-containing molecule, tetrathiafulvalene (TTF), is an ideal candidate due to its small molecular size and low melting point, which makes it ideal for insertion into SWNTs from the liquid phase. When molten TTF and open nanotubes are mixed together, the molecules of TTF become spontaneously inserted into the nanotube cavity (Figure 1b) due to capillary forces. Furthermore, being an electron donor, TTF is known to transfer electrons to the SWNT,[19,20] which provides stabilization for these guest molecules in addition to van der Waals interactions formed with the concave side of the host SWNT. Transmission electron microscopy (TEM) reveals the successful encapsulation of TTF within the confines of the nanotube (Supporting Information). Subsequent thermal treatment (heating under argon at 1000 °C in a sealed quartz vessel) or 80 keV electron beam irradiation (carried out *in situ* during TEM measurements) results in decomposition of the TTF molecules into carbon and sulfur-containing fragments. Under such harsh conditions, decomposed molecules are expected to form structurally poorly defined oligomers or polymers. Indeed, when free unconfined TTF is subjected to the same treatment (1000 °C under argon), the molecules transform into essentially structureless materials, where carbon and sulfur atoms are seemingly distributed randomly (Supporting Information). However, confinement in the nanotube channel imposes strict control on the reaction products, leading to the formation of sulfur-terminated graphene nanoribbons (S-GNR; Figure 1c). Most importantly, the structure of the S-GNR edge is precisely defined at the atomic level, which is crucial for the electronic properties of nanoribbons as demonstrated by our calculations shown below.

The fact that the resultant S-GNRs are qualitatively indistinguishable by TEM (Figure 2), regardless of the source of activation energy (thermal energy at 1000 °C or the kinetic energy of 80 keV electrons at ambient temperature), indicates that the nanoribbons are the thermodynamically most favored product when carbon and sulfur are present within the nanotube.

We find that in the absence of sulfur the decomposition of guest molecules at ~1000 °C typically results in the formation of an internal nanotube within the host SWNT,[21−25] even if other elements, which in theory have the potential to terminate the dangling bonds of edge of GNRs, such as hydrogen, oxygen, nitrogen are present.[26−29] However, it has been

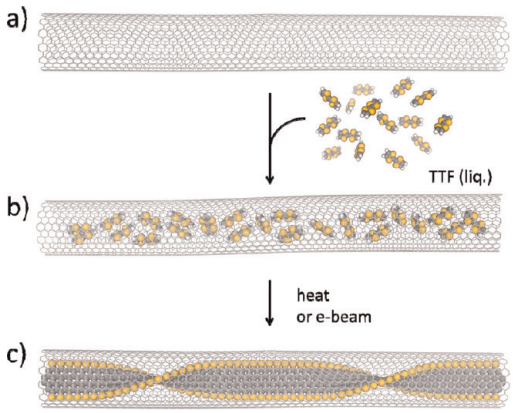

Figure 1. Scheme detailing the synthesis of S-GNRs@SWNT; (a) open, freshly annealed SWNTs are exposed to molten tetrathiafulvalene at 150 °C, which enters the internal cavity of the nanotubes as a liquid; (b) molecules condense inside the nanotube to give the composite structure TTF@SWNT, which is washed with solvent (THF) to remove any molecules from the external surface of the nanotube; (c) upon thermal treatment under argon or e-beam irradiaition in vacuum, the TTF molecules decompose and transform into sulfur-terminated graphene nanoribbons confined within the host SWNT. Systematic AC-HRTEM imaging (discussed below) shows that the S-GNRs are always twisted, as illustrated in model (c).

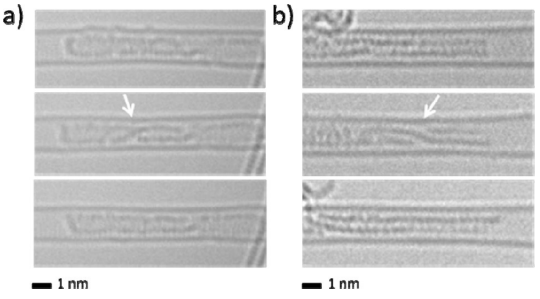

Figure 2. Time series (top to bottom) of 80 kV AC-HRTEM images showing (a) an initial image of a thermally generated S-GNR (1000 °C under argon) and (b) an e-beam-generated S-GNR, both of which are observed to twist and untwist within the nanotube. White arrows indicate the twist in the nanoribbon structure formed reversibly by the S-GNR over time. No discernible difference in the resultant structure of S-GNRs formed by the two methods (heating or e-beam irradiation) is observed by AC-HRTEM.

recently reported that polyaromatic hydrocarbons, such as coronene and perylene, undergo oligomerization within SWNTs at significantly lower temperatures (*e.g.*, 500 °C), which can also lead to nanoribbon formation.[30] In this case, nanoribbons are terminated with hydrogen atoms (H-GNR), but their edges appear to be less well-defined than in the case of S-GNR, probably because the formation process of H-GNR is directly related to the structure and intermolecular orientations of the precursor molecules (polyaromatic hydrocarbons).[30] In contrast, the formation of S-GNR in our experiments appears to be uninfluenced by the structure or exact chemical composition of the molecular precursors since S-GNRs readily form not only from TTF but also from TTF mixtures with C_{60} or fullerenes

functionalized with sulfur-containing groups.[18] The presence of sulfur enables atomically smooth, uniform edges in the resultant S-GNR. It is interesting that tiny quantities of sulfur in a chemical vapor deposition (CVD) reaction mixture were previously found to promote the formation of multilayered stacks of nanoribbons (widths of 20−300 nm)[31] and facilitate nanotube growth[32]—phenomena that may also be related to the effective edge stabilization in graphene nanostructures provided by S atoms. The harsh conditions of nanoribbon formation in our experiments, where precursor molecules are expected to break down into atoms or small clusters of atoms (*e.g.*, C_2, S_2, CS_2, or similar) prior to the assembly of S-GNRs, are not dissimilar to the conditions of CVD.

Aberration-corrected high-resolution TEM (AC-HRTEM) is an excellent technique which allows one to study the formation of new molecular products inside nanotubes, as it provides direct evidence of the location of the encapsulated species. Bulk characterization methods, such as Raman spectroscopy or X-ray diffraction, also provide valuable structural information but do not always offer unambiguous evidence for the presence of the guest structures in SWNTs (as opposed to being adsorbed on the SWNT exterior), and therefore, interpretation of results of any bulk measurements for nanotubes requires care. Our systematic AC-HRTEM imaging reveals that S-GNRs are formed efficiently both *ex situ*, under thermal treatment (Figure 2a), and *in situ*, under electron beam irradiation at 80 keV (Figure 2b). The edges of the nanoribbons are terminated by two dark-atom lines running parallel to each other within the nanotube interior and exhibiting helical twists in certain positions (Figure 2). The edge termination is provided by sulfur atoms, as confirmed by image calculations (qualitative fit between experiment and simulation is shown in Figure 3d,e). In our samples, only sulfur has an atomic number high enough ($Z = 16$) to explain the observed contrast. The other possible edge atoms present in the nanotube (hydrogens) show significantly lower edge contrast (Figure 3c).[33] The ubiquitous presence of the twist in the nanoribbon structure is the most important characteristic distinguishing GNRs from an internal guest nanotube, which show similar AC-HRTEM contrast, or any other polymeric or amorphous products that may form within the host SWNT structure.[18] Only GNRs can have well-defined twists in their structures which are imposed by the confinement, as predicted by theoretical studies.[34,35] Therefore, we consider the helical twist, a structural feature impossible for a guest nanotube to adopt, to be an essential signature of GNR@SWNT systems enabling their definitive identification by AC-HRTEM.

It is expected that the size and structure of the generated S-GNR is governed entirely by the internal diameter of the host nanotube, which should allow precise control over the nanoribbon structure simply by utilizing nanotubes with the appropriate internal channels as templates. To explore the structural diversity of S-GNRs, we employed carbon nanotubes with a range of internal diameters as nanoscale reaction vessels and templates for the formation of nanoribbons.

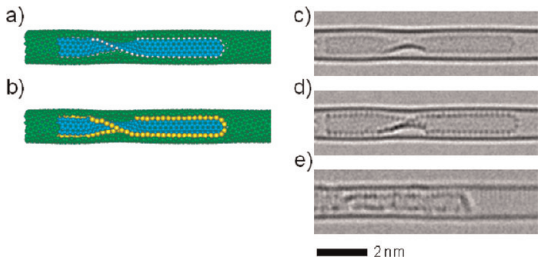

Figure 3. Calculated HRTEM images of (c) H- and (d) S-terminated GNRs inside a SWNT and the corresponding models (a) and (b). The experimental image (e), presented for visual comparison, shows that the contrast of the nanoribbon edge matches the model with sulfur atoms (b,d) closer than the model with hydrogen atoms (a,c).

Following the method described above (Figure 1), S-GNRs were generated in a variety of single-, double-, and triple-walled nanotubes (CNTs). The internal diameters of these host CNTs vary between 0.7 and 4 nm, thus providing numerous degrees of confinement for nanoribbon formation. AC-HRTEM imaging estimates high filling rates (*ca.* 50%) for all nanotubes throughout the sample, with material located solely within the internal cavity (Figure 4). Moreover, many examples show S-GNRs extending parallel to the CNT axis with their length only limited by the length of the nanotube container. Indeed, S-GNRs are observed abundantly inside nanotubes with internal diameters between 1 and 2 nm (Figure 4b−e). Time series AC-HRTEM images (Supporting Information PDF and video files) allow the visualization of the nanoribbons twisting and straightening over time, thus indicating no covalent bonding between the guest GNR and the host CNT and confirming that these structures are definitely nanoribbons rather than internal nanotubes or amorphous structures. As a general trend, the width of the resultant S-GNR is observed to increase proportionally with the internal diameter of the host nanotube (Table 1 and Figure 4).

However, very narrow nanotubes ($d_{NT} < 1$ nm) and very wide nanotubes ($d_{NT} > 2$ nm) appear to contain non-nanoribbon structures, which is indicated by the absence of the characteristic helical twist. The narrow channels of CNTs with internal diameters below 1 nm (*e.g.*, Figure 4a) do not provide sufficient room to accommodate a ribbon-like structure, which can be judged by the absence of the typical twist. The contrast observed within such a narrow CNT originates from atomic chains, similar to those observed for polyyne compounds,[36] possibly incorporating sulfur atoms. Similarly, no evidence of S-GNRs was observed in CNTs with an internal diameter of above 2 nm with either

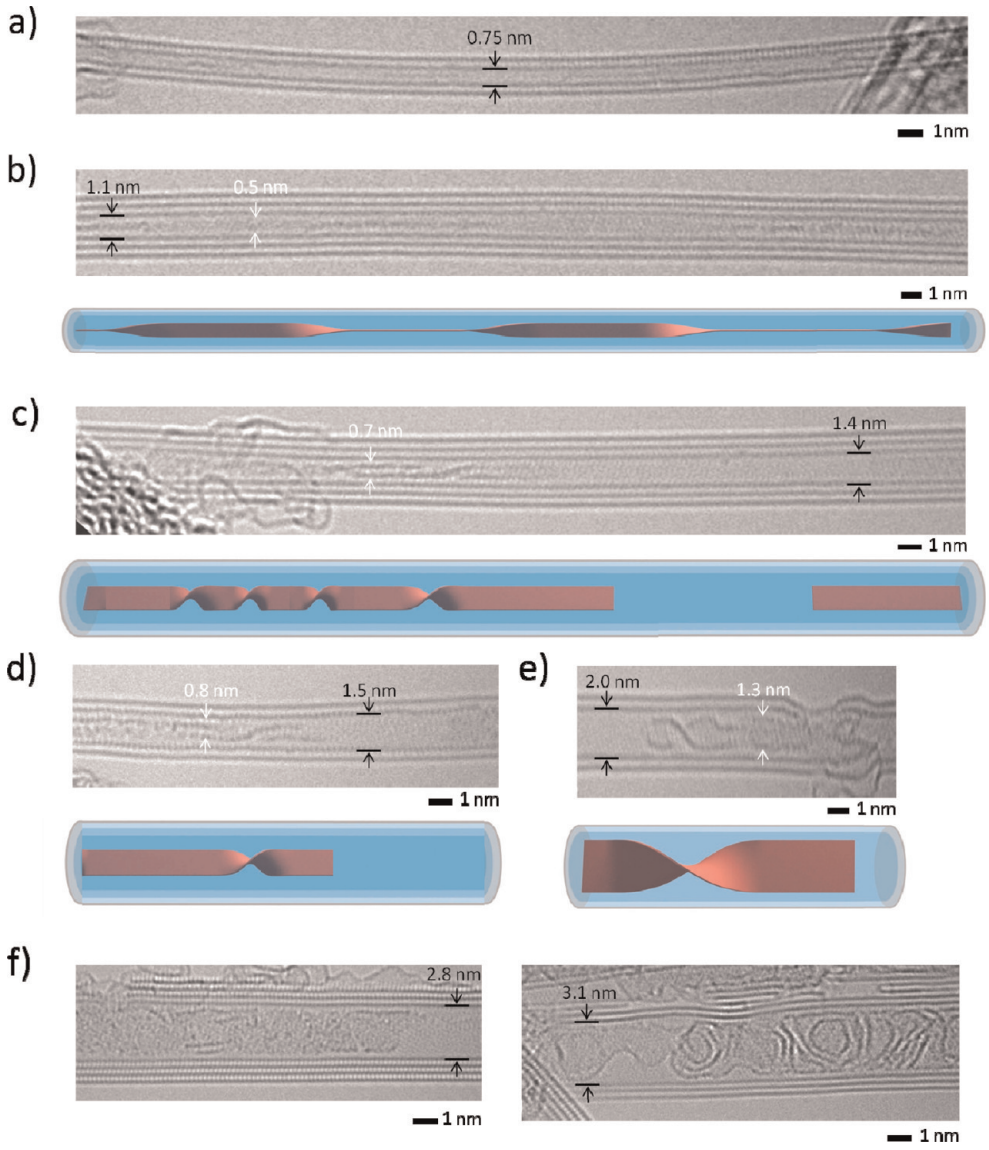

Figure 4. AC-HRTEM images (80 kV) showing the effects of the nanotube internal diameter on the structure of the products formed inside CNTs. (a) Narrow carbon nanotube (internal d_{NT} = 0.75 nm) containing a chain of atoms rather than a S-GNR. (b–e) Nanotubes with internal diameters in the range of d_{NT} = 1–2 nm consistently contain S-GNRs, which exhibit helical twists (indicated by the schematic representation under each image; the nanoribbon and nanotube are depicted in red and blue, respectively). (f) Wide carbon nanotubes (left internal d_{NT} = 2.8 nm and right internal d_{NT} = 3.1 nm) contain structurally poorly defined, semi-amorphous structures (left image) and carbon "onions" (right image) as the host nanotubes are too wide to efficiently template nanoribbon formation.

TABLE 1. Correlation between the Internal Diameters of the Host Nanotubes and the Structures Formed in Their Cavities Measured by TEM

CNT diameter/nm	structure formed	S-GNR width/nm	twist length/nm
0.7	atomic chain		
1.1	nanoribbon	0.5	4.5
1.4	nanoribbon	0.7	2.3
1.5	nanoribbon	0.8	1.8
2.0	nanoribbon	1.3	1.4
2.8	amorphous material		
3.1	nano-onion		

amorphous (d_{NT} = 2–3 nm) or nano-onion (d_{NT} > 3 nm) structures observed instead of nanoribbons (Figure 4f). The lack of confinement in wider CNTs makes them less efficient templates which are not able to direct the growth of nanoribbons. These observations demonstrate the importance of efficient contact between the guest nanoribbon and the concave surface of the host nanotube. Thus, we are able to determine the optimum CNT diameter range of 1–2 nm, which allows both sufficient room for GNR formation while providing a strong templating effect for their unidirectional growth.

Density functional theory (DFT) analysis of different structural models of S-GNRs commensurate with the internal channels of the host nanotubes used in our experiments provides further insight into the nature of

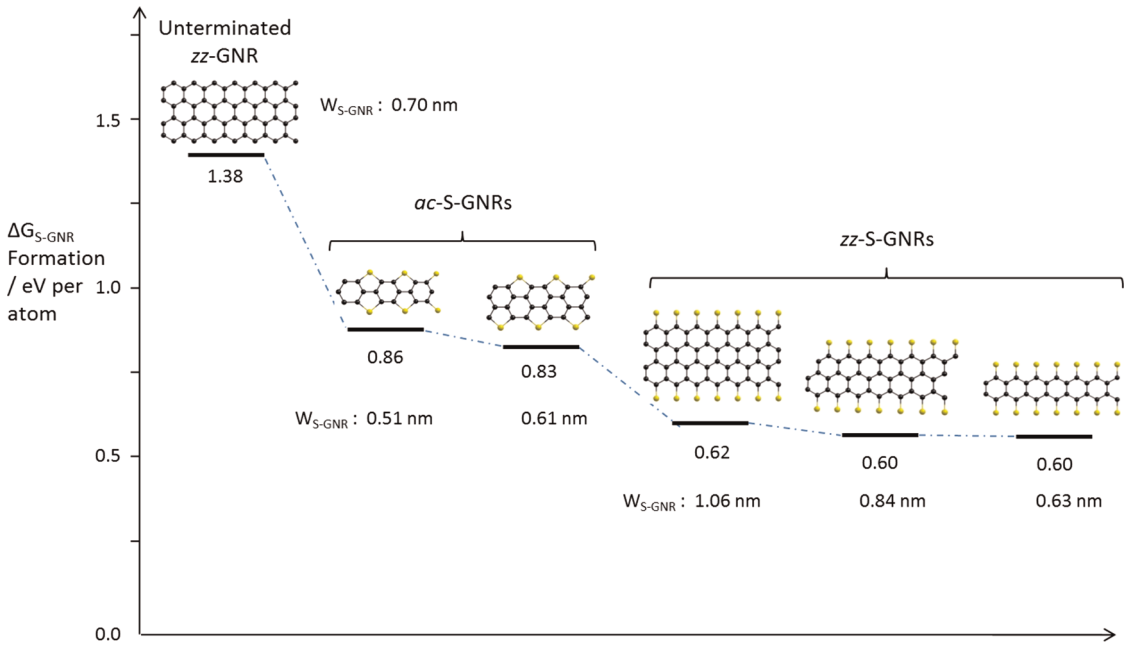

Figure 5. Predicted widths and the ΔG free energies of formation (per atom in eV with respect to graphite; ΔG = 0 eV for graphite) for unterminated GNRs, and different *zz*- S-GNRs and *ac*-S-GNRs.

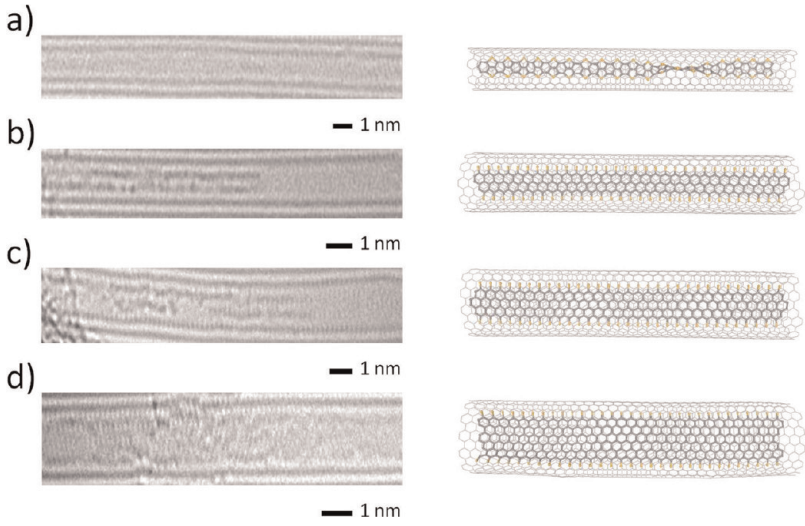

Figure 6. (Left) AC-HRTEM images (80 kV) of S-GNR with widths of (a) 0.49 nm, (b) 0.70 nm, (c) 0.81 nm, and (d) 1.30 nm formed inside carbon nanotubes with internal diameters of (a) 1.1 nm, (b) 1.4 nm, (c) 1.5 nm, and (d) 2.0 nm, respectively, and (right) their structural diagrams.

nanoribbons. Our calculations of the Gibbs free energy of formation, ΔG (eV per atom), for the various S-GNR structures clearly indicate that any sulfur-terminated nanoribbons are significantly more stable than unterminated nanoribbons of a similar width (Figure 5). The key reason for this increase in stability of S-GNRs is related to the removal of the unsaturated valences of the carbon atoms at the edge of the nanoribbon, which have only two bonds instead of the three that are required for an sp^2-carbon atom, by the introduction of sulfur atoms. Furthermore, the magnitude of the stabilization effect of sulfur termination appears to be dependent on the type of nanoribbon edge. All S-GNRs can be viewed as either polythiaperipolycenes (*i.e.*, S-terminated zigzag edged nanoribbons, *zz*-S-GNRs; Figure 5) or polythiophenes (*i.e.*, S-terminated armchair edged nanoribbons with sulfur atoms bridging between two carbon atoms, *ac*-S-GNRs; Figure 5). DFT calculations predict the *zz*-S-GNRs to be more stable than *ac*-S-GNRs of similar width. The formation of *ac*-S-GNRs, rather than the more stable *zz*-SGNRs, within narrower tubes (internal d_{NT} = 1.1 nm) is stabilized by a superior matching of the internal cavity of the nanotube with the narrower structure of *ac*-S-GNRs (Figure 5).

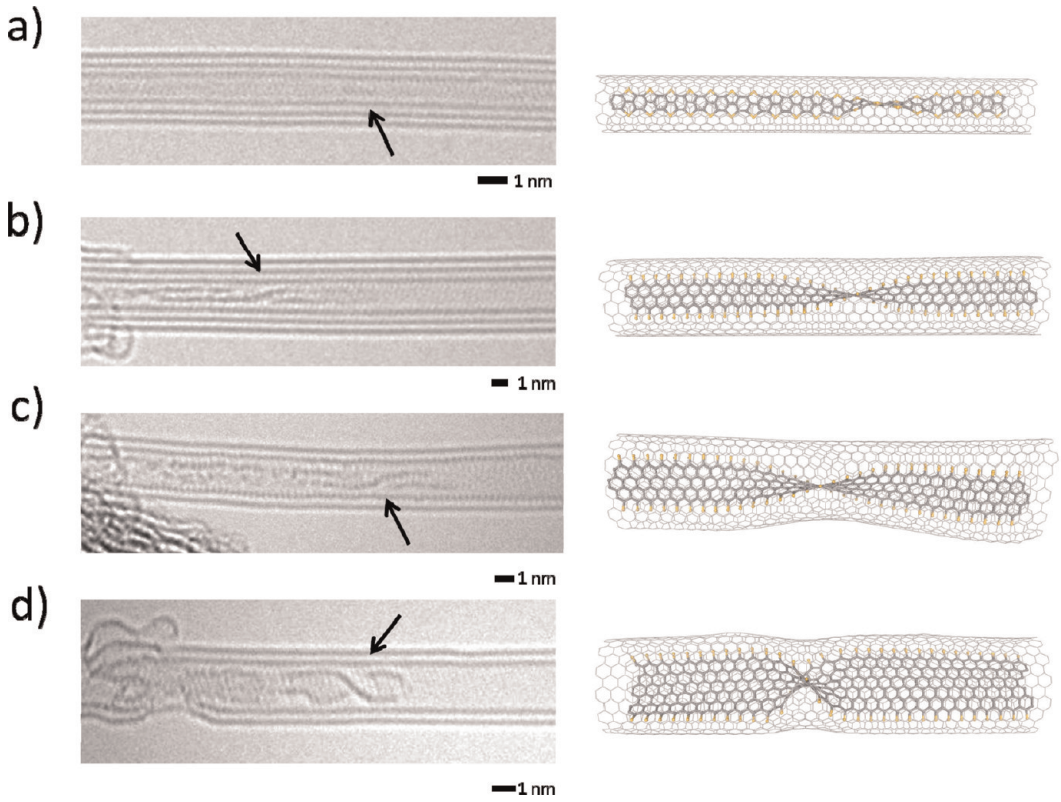

Figure 7. (Left) AC-HRTEM images (80 kV) showing the dependence of the helical pitch of the twisted S-GNR on the width of the nanoribbon within multiwalled carbon nanotubes with internal diameters of (a) 1.1 nm, (b) 1.4 nm, (c) 1.5 nm, and (d) 2 nm. The helical twists in the S-GNRs are indicated with a black arrow in each case. (Right) Corresponding structural diagrams of confined S-GNRs.

Within each class of S-GNRs, there is a very weak dependence of their stability on the width of the nanoribbon, with the Gibbs free energy of formation within approximately 1−3 kJ/mol for nanoribbons containing the same edge structure (Figure 5). Indeed, experimental AC-HRTEM imaging indicates that for *zz*-S-GNRs the host nanotube diameter dictates the number of rows of carbon atoms between the polythiaperipolycene edges, which vary from three to six in the observed examples (Figure 6b−d). For CNTs with narrower internal diameters (*ca.* 1.1 nm), it is more favorable to accommodate *ac*-S-GNRs in the nanotube cavity, and the reduced concentration of sulfur atoms along the S-GNR edges explains their lower contrast in the AC-HRTEM images (Figure 6a). In both cases, the planarity of the S-GNRs is distorted due to interactions with the host CNT and folded into trough-like structures which lead to slightly smaller S-GNR widths observed experimentally in the TEM images (Table 1) as compared to those predicted by DFT (Figure 5). As a result, the S-GNR widths measured by TEM (Figure 6) are consistently smaller than the values calculated for the flat nanoribbons (Figure 5).

S-GNR@CNT systems are highly synergistic: the confinement of the nanoribbon within a nanotube causes the simultaneous distortion of the guest nanoribbon and the host nanotube. Our calculations show that, for a S-GNR with a van der Waals width exceeding the nominal internal diameter of the host nanotube, the strain exerted by the S-GNR can elliptically distort the CNT. The degree of distortion correlates with the width of the S-GNR (Supporting Information). The elliptical distortion of the nanotubes can be observed clearly in time series of TEM images[18] or TEM videos (supporting video files) in which the nanotube diameter is observed to change in response to the orientation of the guest nanoribbon.

Helical twisting of the S-GNR, widely observed in all experimental images of S-GNRs (Figures 2−4, 6, and 7), is another mechanism for alleviating strain in S-GNR@CNT structures. Though such helical twists are invariably observed for all nanoribbons, the periodicity of the twist is seen to decrease as the width of the ribbon increases (Table 1). Similarly, the pitch of the helical twist becomes more pronounced for wider S-GNRs (Figure 7). Both phenomena can be related to the increasing number of carbon−carbon bonds in the S-GNR width capable of absorbing the strain caused by twisting of the ribbon.[34,37] As the nature of the twist in nanoribbons is known to play a significant role in their electronic properties, control over the conformation of GNRs is crucial for their practical applications.[17,38]

The exact mechanism of nanoribbon formation inside nanotubes remains unclear at this stage, as *in situ*

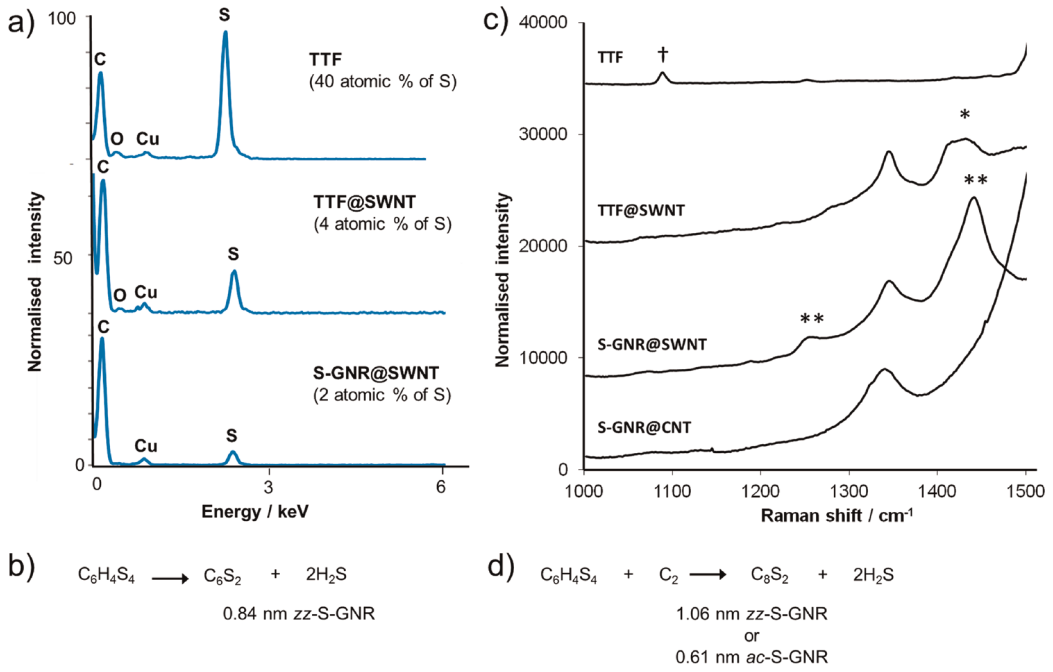

Figure 8. (a) EDX spectra of pristine TTF crystals, TTF inserted in nanotubes (TTF@SWNT), and nanoribbons (S-GNR@SWNT) formed by thermal decomposition of TTF inside nanotubes (atomic percentage of sulfur was determined with respect to the carbon peak; the residual Cu peak is due to the TEM grid). (b) Transformation of TTF ($C_6H_4S_4$) into S-GNRs with zigzag edges and a width of 0.84 nm (*zz*-S-GNR) causes the release of two molecules of hydrogen sulphide. (d) In contrast, the formation of wider *zz*-S-GNR or armchair S-GNR (*ac*-S-GNR) requires additional carbon atoms that can be abstracted from defects in the SWNT at high temperature. (c) Raman spectra of TTF, TTF@SWNT, S-GNR@SWNT (d_{NT} = 1.4−1.6 nm), and S-GNR@CNT (internal d_{NT} = 0.7−3.1 nm) formed at 1000 °C between 1000 and 1500 cm^{-1} show the presence of Raman bands from the encapsulated TTF molecules within the nanotube (*) and the subsequently thermally generated S-GNRs (**). The Raman band of TTF (†) is observed to disappear upon encapsulation within the SWNT.

AC-HRTEM observations indicate that it is a complex and highly dynamic process which is difficult to capture in real time. However, local energy-dispersive X-ray (EDX) spectroscopy, a technique complementary to TEM imaging, enables monitoring of the elemental composition of the structures generated in nanotubes and sheds light on the stoichiometry of S-GNR formation. While EDX does not provide quantitative information about the absolute concentrations of elements, the relative concentrations can be determined accurately and compared for different samples. To avoid EDX signals associated with the substrate (amorphous carbon film), in all EDX measurements, the e-beam was condensed on a part of the specimen hanging over a hole in the TEM grid. The ratio of elements in a crystal of TTF measured by this technique (Figure 8a, top spectrum) was determined to be C/S = 6:4, which is equivalent to a 40 atom % of sulfur (TTF formula = $C_6H_4S_4$) if the hydrogen, which is undetectable by EDX, is disregarded. Similar measurements were carried out for bundles of nanotubes filled with TTF prior to nanoribbon formation (TTF@SWNT) and after nanoribbons were formed by heating at 1000 °C (S-GNR@SWNT). Atoms of the SWNT container contribute most to the intensity of the C peak in the EDX spectra of TTF@SWNT and S-GNR@SWNT (Figure 8a, middle and bottom spectra).

Considering that the typical diameters of the SWNTs in our sample are in the range of 1.3−1.5 nm, 4 atom % of sulfur recorded by EDX corresponds to approximately 50% of the internal volume of the nanotubes being occupied by TTF before heating or e-beam irradiation. After heating at 1000 °C, when nanoribbons are formed inside nanotubes, the concentration of sulfur in the S-GNR@SWNT is reduced by half as compared to the unheated TTF@SWNT sample (Figure 8a). Since the formation of S-GNRs requires only C and S, the hydrogen atoms of TTF are eliminated in the form of hydrogen sulfide gas, which is responsible for the observed reduction of overall sulfur content in the sample. Indeed, considering the stoichiometry of formation of a 0.84 nm wide *zz*-S-GNR (Figure 8b), a structure most compatible with the average diameter of the SWNTs in this sample, shows that two molecules of H_2S are released per each molecule of TTF, which corresponds to the expulsion of half of the total sulfur in the sample and correlates well with EDX measurements. Gaseous H_2S diffuses rapidly out of the SWNT, and its presence in the reaction vessel is detected organoleptically upon S-GNR@SWNT formation. It is clear when considering the stoichiometry for the formation of an armchair nanoribbon, *ac*-S-GNR (Figure 8d), where the concentration of sulfur is lower than in a *zz*-S-GNR of comparable width, or for the formation of any wider *zz*-S-GNRs,

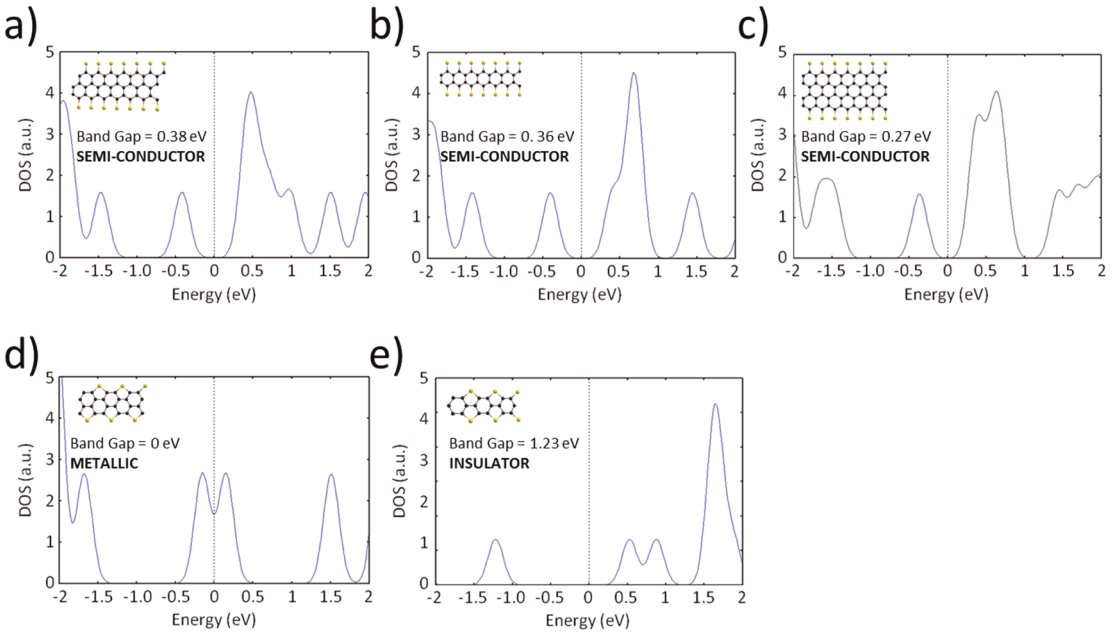

Figure 9. Density of states calculated for *zz*-S-GNRs (a−c) and *ac*-S-GNRs (d,e) of different widths illustrating that electronic properties of sulfur-terminated nanoribbons (semiconductor, metallic, and insulator) are determined by their widths and edge structures.

such as a 1.06 nm *zz*-S-GNR (Figure 8d), that additional carbon atoms are required. The extra carbon can be readily supplied by labile defect sites in the SWNT sidewalls or adventitious carbon ubiquitously present inside nanotubes. Because all carbon nanotubes are intrinsically polydispersed materials, establishing the precise stoichiometry of the nanoribbon formation reactions is not possible at the moment. However, comparative EDX measurements provide useful information about the mechanism of this process.

Since vibrational spectroscopy has previously been utilized for analysis of non-sulfur-terminated nanoribbons,[6,39−42] we investigated S-GNR@SWNT and S-GNR@CNT structures by Raman (Figure 8c) and infrared spectroscopy (Supporting Information). S-GNR@SWNT and S-GNR@CNT samples produced by thermal treatment at 1000 °C showed no bands associated with the vibrations of TTF, thus indicating complete transformation of the guest molecules. The S-GNR@SWNT sample, where nanoribbons are most abundant and structurally uniform, showed the emergence of two new bands, the most distinct of which at *ca.* 1200 cm^{-1} corresponding to the vibrational stretching of C═S bonds[43] at the polythiaperipolycene edge of the *zz*-S-GNRs, confirming the formation of nanoribbons in the bulk. The intensity of this characteristic band is relatively low as compared to the strong bands of the host SWNT, which is consistent with the AC-HRTEM observations that all nanoribbons are encapsulated inside the nanotubes, with no molecular material adsorbed on the CNT surface that would result in much more intense Raman bands as compared to the encapsulated material. The absence of a similarly well-defined band for the C═S bond vibration in S-GNR@CNT samples (Figure 8c, bottom spectrum), in which internal diameters of nanotubes are distributed over a significantly wider range of diameters, most of which are outside the optimum range required for S-GNR formation, is related to a lower abundance of *zz*-S-GNR structures and a larger number of graphitic layers of the host CNT (typically two, three, or several layers) dominating the Raman spectra. As a control, Raman spectra of pure unconfined TTF, thermally treated under the same conditions as those used for the formation of S-GNR in nanotubes, show two peaks at *ca.* 1333 and 1578 cm^{-1}, corresponding to D and G bands of a layered graphitic structure (Supporting Information) but no evidence of a C═S peak at 1200 cm^{-1}, which emphasizes the importance of confinement for the formation of S-GNRs. Furthermore, the presence of S-GNRs in nanotubes has an effect on the vibrations of the host SWNT, resulting in a red shift of the radial breathing mode (RBM) bands measured by Raman spectroscopy (Supporting Information), which may be related to a combined effect of electron transfer from S-GNR to SWNT[18] and mechanical strain in the S-GNR@SWNT system.

Owing to the fact that carbon atoms at the edges of the GNRs have very different bonding characteristics to the carbon atoms in the middle of the nanoribbon, the functional electronic properties of S-GNRs are highly dependent on the precise atomic structure.[44−46] Our DFT calculations show that the electronic band structures for the different S-GNRs vary dramatically from semiconductor in the case of *zz*-S-GNRs to metallic or insulator for the *ac*-S-GNRs (depending on the nanoribbon width; Figure 9). The wealth of electronic properties available in S-GNRs makes them highly versatile 1D materials showing promise for potential applications in electronic and optical devices.

CONCLUSIONS

This study, based on AC-HRTEM imaging, EDX, and Raman spectroscopy and theoretical calculations, demonstrates that carbon nanotubes can act as efficient nanoreactors which template the assembly of sulfur-terminated graphene nanoribbons of different sizes, structures, and conformations. We investigated in detail the formation ranges of S-GNRs under both thermal treatment and electron beam irradiation, demonstrating that nanoribbons are formed efficiently from small sulfur-containing molecules under both conditions. The optimum range of internal diameters for the host CNTs has been determined to be between 1 and 2 nm, which consistently led to the formation of S-GNRs with the nominal widths of 0.5−1.4 nm, corresponding to 3−6 rows of carbon atoms between sulfur-terminated edges. Outside of this range of CNT diameters, graphene nanoribbons do not form.

Theoretical calculations show that the thermodynamic stability of nanoribbons is dependent on the S-GNR edge structure as well as the nanoribbon width. For nanoribbons of similar widths, the polythiaperipolycene-type edges of *zz*-S-GNRs are more stable than the polythiophene-type edges of *ac*-S-GNRs, while for nanoribbons with the same edge structure, their relative stability increases only marginally with increasing width. Both the edge structure and the width define the electronic properties of S-GNRs which can vary widely from metallic to semiconductor to insulator.

The encapsulated nanoribbons exhibit a rich dynamic behavior inside nanotubes, freely rotating within and translating along the nanotube cavity. Helical twists, identified as the definitive structural fingerprint of nanoribbons, form reversibly in S-GNR structures, the pitch of which is seen to be dependent on the width of the nanoribbon, with wider nanoribbons producing a greater helical pitch. The variety and dynamic nature of S-GNR@CNT structures shows promise for the future control of the electronic properties of nanoribbons, which are profoundly affected by the GNR conformation.

EXPERIMENTAL SECTION

TTF@CNT Preparation. Freshly annealed CNTs (Timesnano, arc discharge, heated at 570 °C for 20 min with a weight loss of ~20%) were added immediately to liquid tetrathiafulvalene (20 mg) at 150 °C under an argon atmosphere. The suspension was stirred for 3 h, allowed to cool, and diluted with tetrahydrofuran (2 mL) and filtered onto a PTFE filtration membrane (pore size 0.5 μm). The material was then washed successively with tetrahydrofuran (10 mL) and methanol (10 mL) and dried in air. A sample of TTF@SWNT was prepared using SWNT (5 mg, NanoCarbLab SWNT, arc discharge) using identical conditions.

Thermally Activated Formation of S-GNR. Samples of TTF@CNT and TTF@SWNT were sealed in quartz tubes under ambient pressure of argon (1.01 bar). The tubes were heated at 1000 °C (the argon pressure will increase to *ca.* 4.72 bar) for 20 min, cooled rapidly by submerging the sample in iced water, and opened. HRTEM analysis indicated that comparison of the resultant structures with samples prepared by e-beam irradiation showed no discernible difference.

HRTEM Imaging. Prior to TEM imaging, the nanotubes were dispersed on lacey carbon grids (Agar Scientific). The TEM samples were heated at 140 °C for 10 min in air to reduce contamination during TEM investigation. AC-HRTEM investigation was performed on a FEI Titan 80-300 TEM equipped with an aberration corrector for the objective lens. The TEM was operated at 80 kV. The Schottky-type electron source was operated at a reduced extraction voltage of 2000 V and manually adjusted gun lens excitation of 780 V to reduce the energy spread from 0.7 eV (standard settings) to 0.4 eV to minimize the dampening by the temporal incoherence envelope, which increased the information limit to 0.12 nm.[47,48] Geometric aberrations of second and third order were reduced *via* tuning the imaging corrector to a phase plate of about 20 mrad. The free aberration parameter, C_S, was chosen to be slightly positive (5 μm) and defocus, Δf, to be negative (around −4 to −10 nm) which resulted in dark-atom contrast. Images were acquired onto a Gatan Ultrascan XP slow scan CCD camera using binning 2 (frame size 1k × 1k) and exposure times ranging from 0.25 to 1 s (depending on the vibrations of the tube due to irradiation). The dose rates during HRTEM imaging were between 10^6 and 10^7 e^-/nm^2/s.

EDX Spectroscopy. Local EDX spectra were acquired for samples mounted on TEM grids using an Oxford Instruments INCA X-ray microanalysis system. The electron beam was condensed onto areas of specimens (TTF crystals or nanotube bundles) hanging over holes of the amorphous carbon film to avoid EDX signals of the substrate (illuminated area *ca.* 5 nm in diameter). Quantitative measurements performed for 8−10 different areas of each specimen show only slight variations (±0.5%) in the atomic percentages of C and S, which were determined from the intensities of their EDX peaks at 0.3 and 2.3 keV, respectively.

TEM Image Simulation. The HRTEM images in Figure 3 were simulated using MUSLI multislice code.[49] Coherent aberrations corresponding to those in the experimental images were used. Parameters for the dumping envelope were as follows: focal distance = 1.5 mm (tabulated value for Titan 80-300), coefficient of chromatic aberration = 1.5 mm,[48] energy spread of electron source = 0.4 eV (fwhm, measured experimentally), stability of high tension $\delta U/U = 10^{-6}$ (tabulated value for Titan 80-300), stability of objective lens current $\delta I/I = 3 \times 10^{-7}$ (fitted by simulations). The sampling rate was 0.015 nm/pixel. Images were calculated at an electron dose of 10^6 e^-/nm^2 and further processed using the same routine as for experimental images. Atomistic models for the image simulations were optimized using MM+ empirical potentials including van der Waals interactions.

Raman Measurements. The TTF@CNT, S-GNR@SWNT, and S-GNR@CNT samples were separately dispersed in methanol, mounted onto Si(100) supports, and their Raman spectra were recorded at room temperature (HoribaJY LabRAM HR spectrometer, laser wavelength 532 nm). The intensity of the G band was overscaled to resolve inherently weaker peaks below the G band associated with incarcerated foreign matter.

Theoretical Calculations. Geometry optimization and the electronic band structures of the S-GNRs were generated using the CASTEP code (v. 5.5.1). A plane wave basis set with an energy cut off of 500 eV was used. The convergence threshold for energy was 10^{-6} eV. The spin-polarized generalized gradient approximation (GGA) in the form of the PBE functional was used to solve the exchange correlation term in the Kohn−Sham DFT equation. To generate the pseudopotenitals, the internal CASTEP "on-the-fly" formalism was used, in addition to a 45 k-point sampling grid. The geometry of the nanoribbons was fully

relaxed until the force on each of the atoms was less than 0.05 eV/Å.

Conflict of Interest: The authors declare no competing financial interest.

Acknowledgment. We gratefully acknowledge financial support from the European Research Council (ERC), the Royal Society (A.N.K.), the Engineering and Physical Research Council (EPSRC) for funding a Career Acceleration Fellowship EP/G005060/1 (E.B.), the German Research Foundation (DFG), and the Ministry of Science, Research and Arts (MWK) of the state Baden-Württemberg within the Sub-Ångstrøm Low-Voltage Electron Microscopy (SALVE) project.

Supporting Information Available: Additional HRTEM spectroscopy, Raman and infrared spectroscopy, and theoretical calculations are included. This material is available free of charge *via* the Internet at http://pubs.acs.org.

REFERENCES AND NOTES

1. Yang, L.; Park, C.-H.; Son, Y.-W.; Cohen, M. L.; Louie, S. G. Quasiparticle Energies and Band Gaps in Graphene Nanoribbons. *Phys. Rev. Lett.* **2007**, *99*, 186801.
2. Wakabayashi, K. Electronic Transport Properties of Nanographite Ribbon Junctions. *Phys. Rev. B* **2001**, *64*, 125428.
3. Barone, V.; Hod, O.; Scuseria, G. E. Electronic Structure and Stability of Semiconducting Graphene Nanoribbons. *Nano Lett.* **2006**, *6*, 2748–2754.
4. Kosynkin, D. V.; Higginbotham, A. L.; Sinitskii, A.; Lomeda, J. R.; Dimiev, A.; Price, B. K.; Tour, J. M. Longitudinal Unzipping of Carbon Nanotubes To Form Graphene Nanoribbons. *Nature* **2009**, *458*, 872–876.
5. Jiao, L.; Zhang, L.; Wang, X.; Diankov, G.; Dai, H. Narrow Graphene Nanoribbons from Carbon Nanotubes. *Nature* **2009**, *458*, 877–880.
6. Cai, J. M.; Ruffieux, P.; Jaafar, R.; Bieri, M.; Braun, T.; Blankenburg, S.; Muoth, M.; Seitsonen, A. P.; Saleh, M.; Feng, X. L.; *et al.* Atomically Precise Bottom-Up Fabrication of Graphene Nanoribbons. *Nature* **2010**, *466*, 470–473.
7. Jiao, L.; Wang, X.; Diankov, G.; Wang, H.; Dai, H. Facile Synthesis of High-Quality Graphene Nanoribbons. *Nat. Nanotechnol.* **2010**, *5*, 321–325.
8. Shimizu, T.; Haruyama, J.; Marcano, D. C.; Kosynkin, D. V.; Tour, J. M.; Hirose, K.; Suenaga, K. Large Intrinsic Energy Bandgaps in Annealed Nanotube-Derived Graphene Nanoribbons. *Nat. Nanotechnol.* **2011**, *6*, 45–50.
9. Hirsch, A. Unzipping Carbon Nanotubes: A Peeling Method for the Formation of Graphene Nanoribbons. *Angew. Chem., Int. Ed.* **2009**, *48*, 6594–6596.
10. Balandin, A. A.; Ghosh, S.; Bao, W. Z.; Calizo, I.; Teweldebrhan, D.; Miao, F.; Lau, C. N. Superior Thermal Conductivity of Single-Layer Graphene. *Nano Lett.* **2008**, *8*, 902–907.
11. Ritter, K. A.; Lyding, J. W. The Influence of Edge Structure on the Electronic Properties of Graphene Quantum Dots and Nanoribbons. *Nat. Mater.* **2009**, *8*, 235–242.
12. Li, X. L.; Wang, X. R.; Zhang, L.; Lee, S. W.; Dai, H. J. Chemically Derived, Ultrasmooth Graphene Nanoribbon Semiconductors. *Science* **2008**, *319*, 1229–1232.
13. Tapaszto, L.; Dobrik, G.; Lambin, P.; Biro, L. P. Tailoring the Atomic Structure of Graphene Nanoribbons by Scanning Tunnelling Microscope Lithography. *Nat. Nanotechnol.* **2008**, *3*, 397–401.
14. Stampfer, C.; Gutttinger, J.; Hellmueller, S.; Molitor, F.; Ensslin, K.; Ihn, T. Energy Gaps in Etched Graphene Nanoribbons. *Phys. Rev. Lett.* **2009**, *102*, 056403.
15. Ci, L.; Xu, Z. P.; Wang, L. L.; Gao, W.; Ding, F.; Kelly, K. F.; Yakobson, B. I.; Ajayan, P. M. Controlled Nanocutting of Graphene. *Nano Res.* **2008**, *1*, 116–122.
16. Campos, L. C.; Manfrinato, V. R.; Sanchez-Yamagishi, J. D.; Kong, J.; Jarillo-Herrero, P. Anisotropic Etching and Nanoribbon Formation in Single-Layer Graphene. *Nano Lett.* **2009**, *9*, 2600–2604.
17. Jia, X. T.; Campos-Delgado, J.; Terrones, M.; Meunier, V.; Dresselhaus, M. S. Graphene Edges: A Review of Their Fabrication and Characterization. *Nanoscale* **2011**, *3*, 86–95.
18. Chuvilin, A.; Bichoutskaia, E.; Gimenez-Lopez, M. C.; Chamberlain, T. W.; Rance, G. A.; Kuganathan, N.; Biskupek, J.; Kaiser, U.; Khlobystov, A. N. Self-Assembly of a Sulphur-Terminated Graphene Nanoribbon within a Single-Walled Carbon Nanotube. *Nat. Mater.* **2011**, *10*, 687–692.
19. Takenobu, T.; Takano, T.; Shiraishi, M.; Murakami, Y.; Ata, M.; Kataura, H.; Achiba, Y.; Iwasa, Y. Stable and Controlled Amphoteric Doping by Encapsulation of Organic Molecules Inside Carbon Nanotubes. *Nat. Mater.* **2003**, *2*, 683–688.
20. Lu, J.; Nagase, S.; Yu, D. P.; Ye, H. Q.; Han, R. S.; Gao, Z. X.; Zhang, S.; Peng, L. M. Amphoteric and Controllable Doping of Carbon Nanotubes by Encapsulation of Organic and Organometallic Molecules. *Phys. Rev. Lett.* **2004**, *93*, 116804.
21. Bandow, S.; Takizawa, M.; Hirahara, K.; Yudasaka, M.; Iijima, S. Raman Scattering Study of Double-Wall Carbon Nanotubes Derived from the Chains of Fullerenes in Single-Wall Carbon Nanotubes. *Chem. Phys. Lett.* **2001**, *337*, 48–54.
22. Koshino, M.; Niimi, Y.; Nakamura, E.; Kataura, H.; Okazaki, T.; Suenaga, K.; Iijima, S. Analysis of the Reactivity and Selectivity of Fullerene Dimerization Reactions at the Atomic Level. *Nat. Chem.* **2010**, *2*, 117–124.
23. Warner, J. H.; Ito, Y.; Zaka, M.; Ge, L.; Akachi, T.; Okimoto, H.; Porfyrakis, K.; Watt, A. A. R.; Shinohara, H.; Briggs, G. A. D. Rotating Fullerene Chains in Carbon Nanopeapods. *Nano Lett.* **2008**, *8*, 2328–2335.
24. Kitaura, R.; Imazu, N.; Kobayashi, K.; Shinohara, H. Fabrication of Metal Nanowires in Carbon Nanotubes *via* Versatile Nano-Template Reaction. *Nano Lett.* **2008**, *8*, 693–699.
25. Warner, J. H.; Ito, Y.; Rummeli, M. H.; Gemming, T.; Buchner, B.; Shinohara, H.; Briggs, G. A. D. One-Dimensional Confined Motion of Single Metal Atoms Inside Double-Walled Carbon Nanotubes. *Phys. Rev. Lett.* **2009**, *102*, 195504.
26. Fujita, Y.; Bandow, S.; Iijima, S. Formation of Small-Diameter Carbon Nanotubes from PTCDA Arranged Inside the Single-Wall Carbon Nanotubes. *Chem. Phys. Lett.* **2005**, *413*, 410–414.
27. Britz, D. A.; Khlobystov, A. N.; Wang, J. W.; O'Neil, A. S.; Poliakoff, M.; Ardavan, A.; Briggs, G. A. D. Selective Host–Guest Interaction of Single-Walled Carbon Nanotubes with Functionalised Fullerenes. *Chem. Commun.* **2004**, 176–177.
28. Chamberlain, T. W.; Camenisch, A.; Champness, N. R.; Briggs, G. A. D.; Benjamin, S. C.; Ardavan, A.; Khlobystov, A. N. Toward Controlled Spacing in One-Dimensional Molecular Chains: Alkyl-Chain-Functionalized Fullerenes in Carbon Nanotubes. *J. Am. Chem. Soc.* **2007**, *129*, 8609–8614.
29. Chamberlain, T. W.; Meyer, J. C.; Biskupek, J.; Leschner, J.; Santana, A.; Besley, N. A.; Bichoutskaia, E.; Kaiser, U.; Khlobystov, A. N. Reactions of the Inner Surface of Carbon Nanotubes and Nanoprotrusion Processes Imaged at the Atomic Scale. *Nat. Chem.* **2011**, *3*, 732–737.
30. Talyzin, A. V.; Anoshkin, I. V.; Krasheninnikov, A. V.; Nieminen, R. M.; Nasibulin, A. G.; Jiang, H.; Kauppinen, E. I. Synthesis of Graphene Nanoribbons Encapsulated in Single-Walled Carbon Nanotubes. *Nano Lett.* **2011**, *11*, 4352–4356.
31. Campos-Delgado, J.; Romo-Herrera, J. M.; Jia, X. T.; Cullen, D. A.; Muramatsu, H.; Kim, Y. A.; Hayashi, T.; Ren, Z. F.; Smith, D. J.; Okuno, Y.; *et al.* Bulk Production of a New Form of sp^2 Carbon: Crystalline Graphene Nanoribbons. *Nano Lett.* **2008**, *8*, 2773–2778.
32. Motta, M. S.; Moisala, A.; Kinloch, I. A.; Windle, A. H. The Role of Sulphur in Synthesis of Carbon Nanotubes by Chemical Vapour Deposition at High Temperatures. *J. Nanosci. Nanotechnol.* **2008**, *8*, 2442–2449.
33. Meyer, J. C.; Kurasch, S.; Park, H. J.; Skakalova, V.; Kunzel, D.; Gross, A.; Chuvilin, A.; Algara-Siller, G.; Roth, S.; Iwasaki, T.; *et al.* Experimental Analysis of Charge Redistribution Due to Chemical Bonding by High-Resolution Transmission Electron Microscopy. *Nat. Mater.* **2011**, *10*, 209–215.

34. Jiang, Y. Y.; Li, H.; Li, Y. F.; Yu, H. Q.; Liew, K. M.; He, Y. Z.; Liu, X. F. Helical Encapsulation of Graphene Nanoribbon into Carbon Nanotube. *ACS Nano* **2011**, *5*, 2126–2133.
35. Patra, N.; Song, Y. B.; Kral, P. Self-Assembly of Graphene Nanostructures on Nanotubes. *ACS Nano* **2011**, *5*, 1798–1804.
36. Zhao, C.; Kitaura, R.; Hara, H.; Irle, S.; Shinohara, H. Growth of Linear Carbon Chains Inside Thin Double-Wall Carbon Nanotubes. *J. Phys. Chem. C* **2011**, *115*, 13166–13170.
37. Bets, K. V.; Yakobson, B. I. Spontaneous Twist and Intrinsic Instabilities of Pristine Graphene Nanoribbons. *Nano Res.* **2009**, *2*, 161–166.
38. Zhang, D. B.; Dumitrica, T. Effective-Tensional-Strain-Driven Bandgap Modulations in Helical Graphene Nanoribbons. *Small* **2011**, *7*, 1023–1027.
39. Saito, R.; Furukawa, M.; Dresselhaus, G.; Dresselhaus, M. S. Raman Spectra of Graphene Ribbons. *J. Phys.: Condens. Matter* **2010**, *22*, 334203.
40. Gillen, R.; Mohr, M.; Maultzsch, J. Raman-Active Modes in Graphene Nanoribbons. *Phys. Status Solidi B* **2010**, *247*, 2941–2944.
41. Malola, S.; Hakkinen, H.; Koskinen, P. Comparison of Raman Spectra and Vibrational Density of States between Graphene Nanoribbons with Different Edges. *Eur. Phys. J. D* **2009**, *52*, 71–74.
42. Luo, G. F.; Wang, L.; Li, H.; Qin, R.; Zhou, J.; Li, L. Z.; Gao, Z. X.; Mei, W. N.; Lu, J.; Nagase, S. Polarized Nonresonant Raman Spectra of Graphene Nanoribbons. *J. Phys. Chem. C* **2011**, *115*, 24463–24468.
43. Grainger, R. S.; Patel, B.; Kariuki, B. M.; Male, L.; Spencer, N. Sulfur Monoxide Transfer from peri-Substituted Trisulfide-2-oxides to Dienes: Substituent Effects, Mechanistic Studies and Application in Thiophene Synthesis. *J. Am. Chem. Soc.* **2011**, *133*, 5843–5852.
44. Son, Y.-W.; Cohen, M. L.; Louie, S. G. Energy Gaps in Graphene Nanoribbon. *Phys. Rev. Lett.* **2006**, *97*, 216803.
45. Rudberg, E.; Salek, P.; Luo, Y. Nonlocal Exchange Interaction Removes Half-Metallicity in Graphene Nanoribbons. *Nano Lett.* **2007**, *7*, 2211–2213.
46. Hod, O.; Barone, V.; Peralta, J. E.; Scuseria, G. E. Enhanced Half-Metallicity in Edge-Oxidized Zigzag Graphene Nanoribbons. *Nano Lett.* **2007**, *7*, 2295–2299.
47. Meyer, J. C.; Chuvilin, A.; Algara-Siller, G.; Biskupek, J.; Kaiser, U. Selective Sputtering and Atomic Resolution Imaging of Atomically Thin Boron Nitride Membranes. *Nano Lett.* **2009**, *9*, 2683–2689.
48. Haider, M.; Hartel, P.; Müller, H.; Uhlemann, S.; Zach, J. Information Transfer in a TEM Corrected for Spherical and Chromatic Aberration. *Microsc. Microanal.* **2010**, *16*, 393–408.
49. Chuvilin, A.; Kaiser, U. On the Peculiarities of CBED Pattern Formation Revealed by Multislice Simulation. *Ultramicroscopy* **2005**, *104*, 73–82.